King Saud University

Arabian Journal of Chemistry

CrossMark

REVIEW

Mini-review: Ferrite nanoparticles in the catalysis

Boris I. Kharisov [a,*], H.V. Rasika Dias [b], Oxana V. Kharissova [a]

[a] *Universidad Autónoma de Nuevo León, Ciudad Universitaria, Monterrey 66450, Mexico*
[b] *Department of Chemistry & Biochemistry, The University of Texas at Arlington, 700 Planetarium Place, Arlington 76019, Texas, USA*

Abstract Recent applications of ferrite nanoparticles as catalysts in organic processes are reviewed. Catalytic applications include the use of mainly cobalt, nickel, copper, and zinc ferrites, as well as their mixed-metal combinations with Cr, Cd, Mn and sometimes some lanthanides. Core–shell nanostructures with silica and titania are also used without loss of magnetic properties. The ferrite nanomaterials are obtained mainly by wet-chemical sol-gel or co-precipitation methods, more rarely by the sonochemical technique, mechanical high-energy ball milling, spark plasma sintering, microwave heating or hydrothermal route. Catalytic processes with application of ferrite nanoparticles include decomposition (in particular photocatalytic), reactions of dehydrogenation, oxidation, alkylation, C–C coupling, among other processes. Ferrite nano catalysts can be easily recovered from reaction systems and reused up to several runs almost without loss of catalytic activity.
© 2014 The Authors. Production and hosting by Elsevier B.V. on behalf of King Saud University. This is an open access article under the CC BY-NC-ND license (http://creativecommons.org/licenses/by-nc-nd/3.0/).

Contents

* Corresponding author.
  E-mail addresses: bkhariss@hotmail.com (B.I. Kharisov), dias@uta.edu (H.V.R. Dias).

ELSEVIER | **Production and hosting by Elsevier**

1. Introduction

Ferrites are chemical compounds obtained as powder or ceramic bodies with ferrimagnetic properties formed by iron oxides as their main component, Fe_2O_3 and FeO, which can be partly changed by other transition metal oxides (Santina Mohallem, 2012). Among iron oxides and ferrites, *magnetite* (Fe_3O_4) and *maghemite* (γ-Fe_2O_3) are of particular interest. Magnetite is an inverse spinel ferrite. The oxygen ions form a close-packed cubic lattice with the iron ions located at two different interstices between them, tetrahedral (A) sites and octahedral (B) sites. Chemically, magnetite/maghemite can be represented by the formula: Fe^{3+} [Fe_{1-y}^{2+} Fe_{1-y}^{3+} $Fe_{1.67y\square0.33y}^{3+}$]$O_4$, ($\square$ indicates vacancies) where $y = 0$ stays for pure magnetite and $y = 1$ for pure maghemite (fully oxidized magnetite). In the

temperature range from room to Curie temperature ($T_c = 860$ K) the A sites are populated by Fe^{3+} ions and the B sites are populated equally by Fe^{3+} and Fe^{2+} ions. That way, twice as many sites are populated with Fe^{3+} than with Fe^{2+} ions. These and other iron oxide nanoparticles are discussed in our previous review (Kharisov et al., 2012) and are omitted here.

The ferrites can be classified according to their crystalline structure: hexagonal ($MFe_{12}O_{19}$), garnet ($M_3Fe_5O_{12}$) and spinel (MFe_2O_4), where *M* represents one or more bivalent transition metals (Mn, Fe, Co, Ni, Cu, and Zn). Transition metal ferrites, both doped and undoped, are attractive candidates in a wide range of applications including catalysis (Lu et al., 2011), sustainable hydrogen production application (Gaikwad et al., 2011) and electronic and magnetic devices, among
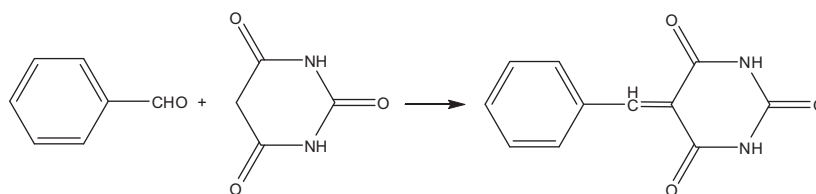
Figure 1 Optimization of reaction conditions using $CoFe_2O_4$ nanocatalyst. Yields 40–95%, best yields were observed in EtOH.
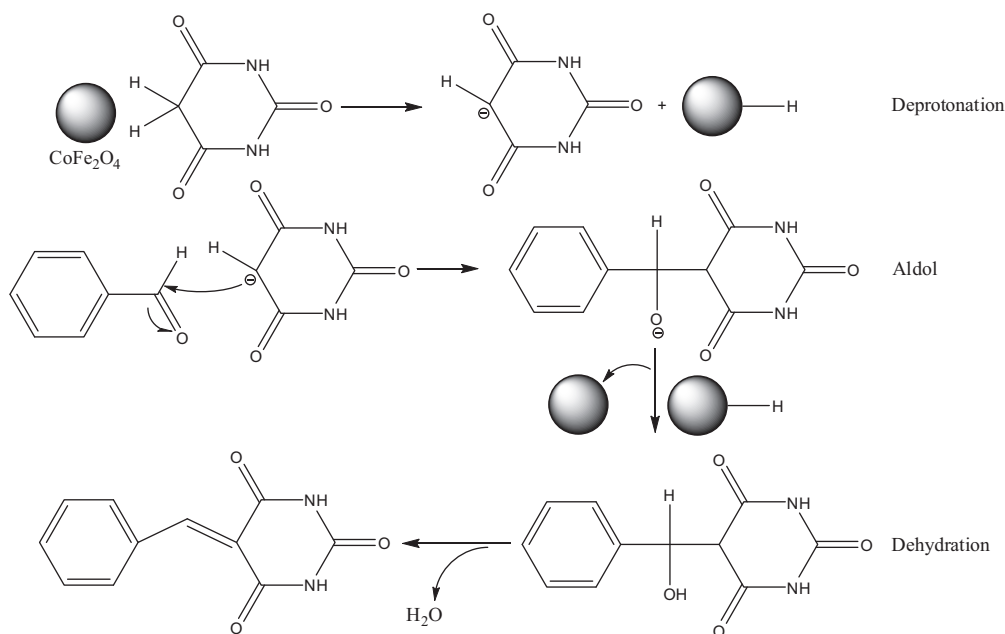
Figure 2 Proposed mechanism for synthesis of arylidene barbituric acid using $CoFe_2O_4$ nanocatalyst.
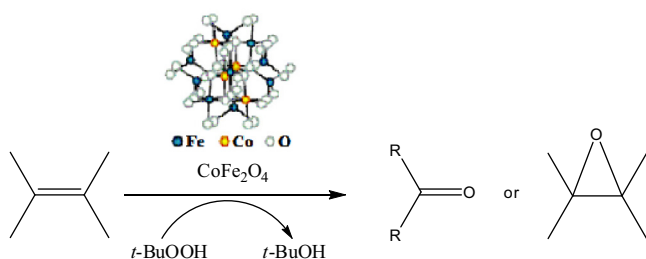
Figure 3 Oxidation of alkenes using $CoFe_2O_4$ catalyst.

Table 1 Effect of solvent on oxidation of styrene catalyzed by $CoFe_2O_4$.[a]

Solvent	Styrene conversion (%)[b]	Selectivity of benzaldehyde (%)
Acetonitrile	10	88
Chloroform	65	55
1,2-Dichloroethane	70	85
Methanol	45	53
1,2-Dichloroethane/ Methanol (1:1)	55	68

[a] Reaction conditions: alkene (1 mmol), t-BuOOH (3 mmol), catalyst (40 mg), solvent (5 mL), $t = 12$ h, $T = 70$ °C.
[b] GC yields based on starting alkenes.

others. Their great advantages for catalytic purposes are that they are generally magnetic and can be easily recovered after completion of reactions using a magnet (Lim and Lee, 2010). For the case of ferrite nanoparticles, up to this moment, only copper, cobalt, nickel, zinc and several mixed-metal and core–shell ferrites are being applied in the catalytic reactions, mainly in processes of the synthesis and destruction of organic compounds. Methods for their preparation are described elsewhere (Kasi Viswanath and Murthy, 2013; Pinheiro Braga et al., 2011; Koferstein, 2013; Gatelite et al., 2011). The synthesis conditions have strongly influenced the crystal structure,

crystallite size, microstructure, magnetic and photocatalytic properties.

Ferrite magnetic nanoparticles (MNPs) and their composites seem to be in near future promising materials for catalytic purposes. In this mini-review, we generalize recent achievements on applications of ferrite nanoparticles in various catalytic reactions.

2. Cobalt ferrites

Cobalt ferrites having different sizes, from ultrasmall 2 nm to 50 nm, can be fabricated by distinct techniques (Goodarz Naseri et al., 2010), mainly the co-precipitation method (CPM), sometimes without using any capping agents/surfactants. Thus, the CPM was used to synthesize ultrasmall $CoFe_2O_4$ superparamagnetic nanoparticles (SPMNPs, 2–8 nm of an average size and high surface area of 140.9 m²/g) without any surfactant (Kaur Rajput, 2013). Their catalytic activity was verified in the synthesis of arylidene barbituric acid derivatives (Figs. 1 and 2) using $CoFe_2O_4$ SPMNPs as a magnetically separable and reusable catalyst in aqueous ethanol. The advantages of this protocol were very short reaction time, high yields, high turnover frequency, simple work-up procedure, economy, a clean reaction methodology, and chemoselectivity, as well as provision of an ecofriendly and green synthesis. More large-size $CoFe_2O_4$ magnetic nanoparticles (25 nm) were used as a catalyst for the oxidation of various alkenes in the presence of $tert$-butylhydroperoxide (t-BuOOH) with almost quantitative yields (Fig. 3) (Kooti and Afshari, 2012). It seemed that this heterogeneous catalysis system proceeds by coordination of t-BuOOH to the metal (Fe^{3+} cations) on the surface of the catalyst. The separation of the catalyst from the reaction media was easily achieved with the aid of an external magnet, and the catalyst can be reused several times with no loss of activity. As an example, effect of solvent on oxidation of styrene catalyzed by $CoFe_2O_4$ is shown in Table 1. In addition, combination of synthesis techniques can also be used for cobalt ferrite preparation. Thus, synthesis of spinel
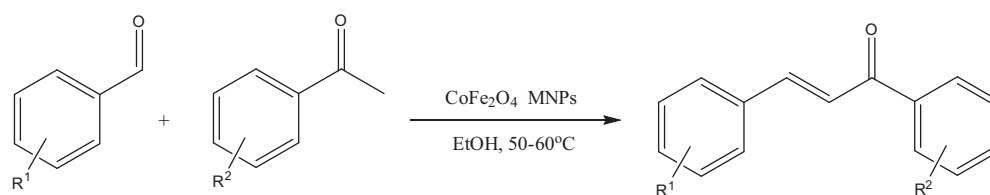
Figure 4 Aldol condensation reaction in the presence of $CoFe_2O_4$ MNPs.
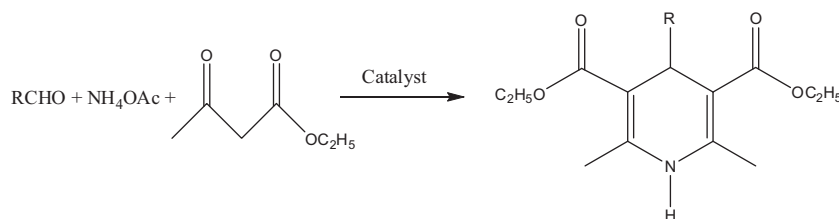
Figure 5 Reaction of substituted aromatic aldehydes, ethyl acetoacetate and ammonium acetate in the presence of $CuFe_2O_4$ (1 mol.%), R= (a) Ph, (b) 4-Me-o-C_6H_4, (c) 4-ClC_6H_4, (d) 4-NO_2-C_6H_4, (e) 4-MeC_6H_4, (f) 3-NO_2-C_6H_4, (g) n-C_9H_9, (h) 2-NO_2-C_6H_4, (i) 2-furyl, (j) 2-Me-o-C_6H_4.

$CoFe_2O_4$ MNPs (average sizes 40–50 nm) was achieved by the combined sonochemical and co-precipitation technique in aqueous medium, also without any surfactant or organic capping agent (Kamal Senapati and Phukan, 2011). These uncapped NPs (nanoparticles) were utilized directly for aldol reaction in ethanol (Fig. 4). After the reaction was over, the nanoparticles were compartmented by using an external magnet.

3. Nickel ferrites

Pure or doped nickel ferrites out of the nano-range size are common and frequently used in several catalytic processes. For instance, high reactivity of $NiFe_2O_4$ (1 1 1) surfaces (higher that in Fe_3O_4) is well-known; $NiFe_2O_4$ is an effective metal-doped ferrite catalyst in a typical industrial process such as the water–gas shift (WGS) reaction (Kumar et al., 2013). Similarly, $NiFe_2O_4$ was examined as a catalyst in photocatalytic water oxidation using $[Ru(bpy)_3]^{2+}$ as a photosensitizer and $S_2O_8^{2-}$ as a sacrificial oxidant (Hong et al., 2012). The catalytic activity of $NiFe_2O_4$ is comparable to that of a catalyst containing Ir, Ru, or Co in terms of O_2 yield and O_2 evolution rate under ambient reaction conditions. As an example of non-nano-sized doped ferrites, their catalysts (granules of ~1 mm diameter) of nickel, cobalt and copper, prepared by co-precipitation hydrothermal route and impregnated with palladium, cerium and lanthanum as promoters (Radhakrishnan Nair and Aniz, 2013), were tested for carbon monoxide oxidation activities.

At the same time, nanosize-range pure nickel ferrites are not yet widely applied for catalytic purposes. As a unique example, ultrasmall spinel oxide $NiFe_2O_4$ particles (3–8 nm in size) were prepared by the combination of chemical precipitation and subsequent mechanical high-energy ball milling from metal nitrates as precursors (Manova et al., 2007). These procedures resulted in the formation of nanocrystalline nickel ferrite, where the particle size can be controlled by the treatment time. Their catalytic behavior in methanol decomposition to CO and methane was tested, showing differences in the phase composition and catalytic behavior depending on the preparation method used. In addition, an interesting observation was made for non-stoichiometric nickel ferrites: the electrocatalytic activity of nickel ferrite NPs for hydrogen evolution reaction was found to increase in the order of $Fe_3O_4 \leqslant Ni_{0.6}Fe_{2.4}O_4 < Ni_{0.2}Fe_{2.8}O_4 \leqslant Ni_{0.8}Fe_{2.8}O_4 < Ni_{0.4}Fe_{2.6}O_4$ (Abbaspour and Mirahmadi, 2013).

4. Copper ferrites

Non-nanosized range copper ferrites have certain catalytic applications, such as, for example, for CO conversion to CO_2 (Lou, 2006). In a difference of pure nickel ferrites, copper ferrite NPs are applied in organic catalysis in more uniform particle size (mainly about 20 nm). Thus, copper ferrite nano material (20 nm) was used as reusable heterogeneous initiator in the synthesis of 1,4-dihydropyridines. The reaction of substituted aromatic aldehydes, ethyl acetoacetate and ammonium acetate (Fig. 5) was achieved in the presence of copper ferrite nano powders at r.t. (room temperature) in ethanol. The nano catalyst was easily recovered and its reusability was confirmed (Kasi Viswanath and Murthy, 2013). The same 20 nm size copper ferrite nano material also was reported as reusable
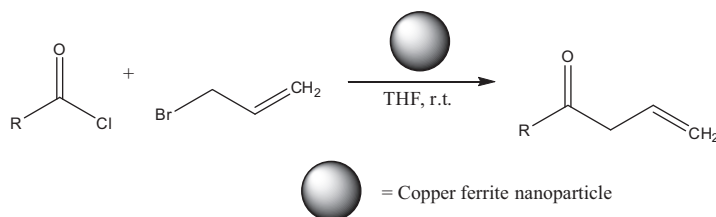
Figure 6 Synthesis of β,γ-unsaturated ketone using allyl bromide. R = (a) C_6H_5, (b) 2-ClC_6H_4, (c) 2-Br, 5-F, C_6H_3, (d) 2-Br, 5-F, C_6H_3, (e) furanyl, (f) 5-phenyl, 3-Methyl, 4-Isoxazolyl, (g) 5-(2,5-dichloro)phenyl, 3-methyl, 4-isoxazolyl, (h) $(CH_3)_3C$-, (i) $C_{11}H_{23}$-, (j) $C_{15}H_{31}$-.
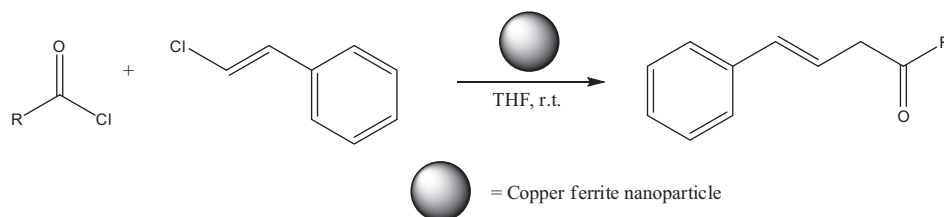
Figure 7 Synthesis of β,γ-unsaturated ketone using cinnamyl chloride. Synthesis of β,γ-unsaturated ketone using cinnamyl chlorides. R= (a) C_6H_5, (b) 2-ClC_6H_4, (c) furanyl, (d)-$CH(CH_3)_2$.
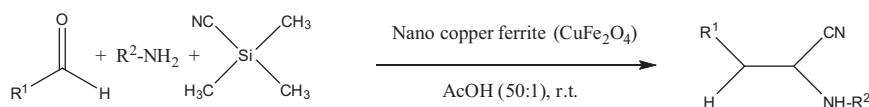
Figure 8 The synthesis of α-aminonitriles in the presence of nano $CuFe_2O_4$ in water as green solvent at r.t.

heterogeneous initiator in the synthesis of β,γ-unsaturated ketones and allylation to acid chlorides in THF at r.t. without any additive/co-catalyst (Figs. 6 and 7) (Murthy et al., 2012). The notable advantages are less expensive, heterogeneous reusable catalyst; mild reaction conditions, high yields of products, shorter reaction times, no isomerization during the reaction and easy workup. In addition, 20 nm $CuFe_2O_4$ was applied as reusable heterogeneous initiator in the synthesis of α-aminonitriles by one-pot reaction of different aldehydes with amines and trimethylsilyl cyanides at r.t. in water as a solvent (Figs. 8 and 9) (Gharib, 2014). α-Aminonitriles are important in preparing a wide variety of amino acids, amides, diamines, and nitrogen containing heterocycles. Also, spherical cubic spinel $CuFe_2O_4$ "oversized" nanostructures (size 116 nm; band-gap energy 1.69 eV) revealed enhanced photocatalytic activity in the conversion of benzene under Xe lamp irradiation (Shen et al., 2013).

Larger-size cubic copper ferrite $CuFe_2O_4$ nanopowders (24–51 nm in size) were synthesized via a hydrothermal route using industrial wastes (ferrous sulfate containing free sulfuric acid $\approx 10\%$, 0.01% Zn^{2+} and 2% silica; copper waste 12.5% Cu, 8.7% Cl^- with minor Ni 0.001%) (Rashad et al., 2012). It was revealed that a single phase of cubic copper ferrite powders can be obtained at different temperatures from 100 to 200 °C for times from 12 to 36 h with pH values 8–12. The microstructures of the produced powders were affected with the synthesis conditions. The particles appeared as nanospheres at hydrothermal temperature 150 °C, hydrothermal time 12 h and pH 8 which changed to the pseudo-cubic-like structure at hydrothermal temperature 200 °C, hydrothermal time 12 h and pH 8. Study of photocatalytic degradation of the methylene blue (MB, $C_{16}H_{18}ClN_3S$) dye using copper ferrite powders showed a good catalytic efficiency (95.9%) at hydrothermal temperature 200 °C for hydrothermal time 24 h at pH = 12 due to the high surface area (118.4 m^2/g).

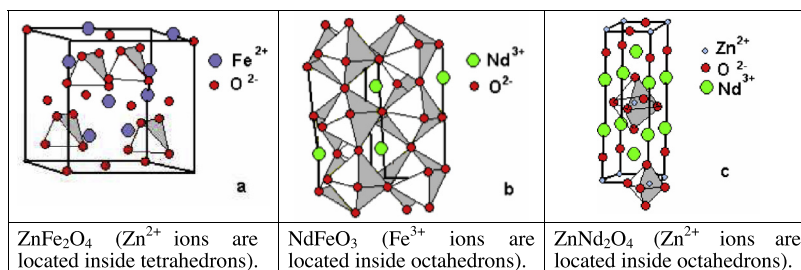## 5. Zinc ferrites

Non-nano-sized zinc ferrites ($ZnFe_2O_4$) have been used in oxidative organic reactions. Thus, the catalytic behavior for oxidative conversion of methane and oxidative coupling of methane was investigated over pure and neodymium substituted zinc ferrites (Fig. 10) prepared by the combustion method (Papa et al., 2010). The catalytic activity proved to be strongly related to the oxide structure as well as to the specific defects created by substitution. The pure zinc ferrite ($ZnFe_2O_4$) and $ZnNd_2O_4$ exhibited high activity for the coupling reaction whereas the neodymium substituted ferrites ($ZnFe_{1.75}Nd_{0.25}O_4$, $ZnFe_{1.5}Nd_{0.5}O_4$ and $ZnFeNdO_4$) were low active in this reaction. The order of the catalytic activities expressed as yields to C_2^+ were $ZnNd_2O_4 > ZnFe_2O_4 > ZnFe_{1.75}Nd_{0.25}O_4 > ZnFeNdO_4 > ZnFe_{1.5}Nd_{0.5}O_4$.

Analyzing pure zinc ferrite nanocatalysts, we note that mainly ultrasmall particles are currently applied in catalytic purposes. Thus, a nanosized highly ordered mesoporous zinc ferrite (ZF, 7–10 nm in size) was synthesized via the co-precipitation method, further sulfated with ammonium sulfate solution to obtain sulfated ZF (SZF) and was used for the synthesis of nopol by Prins condensation of β-pinene and paraformaldehyde (Figs. 11 and 12) (Jadhav et al., 2012). 70% conversion of β-pinene with 88% selectivity to nopol was observed; the spent catalyst was regenerated and reused successfully up to four cycles with a slight loss in catalytic activity. The influence of various reaction parameters such as solvent, reaction temperature, effect of substrate stoichiometry and catalyst loading was investigated. In particular, very low conversion (9%) of β-pinene was observed in protic solvents such as methanol (solvent effect); in the case of apolar–aprotic solvents such as hexane, ethyl acetate and toluene, increase in the β-pinene conversion as well as nopol selectivity was observed.
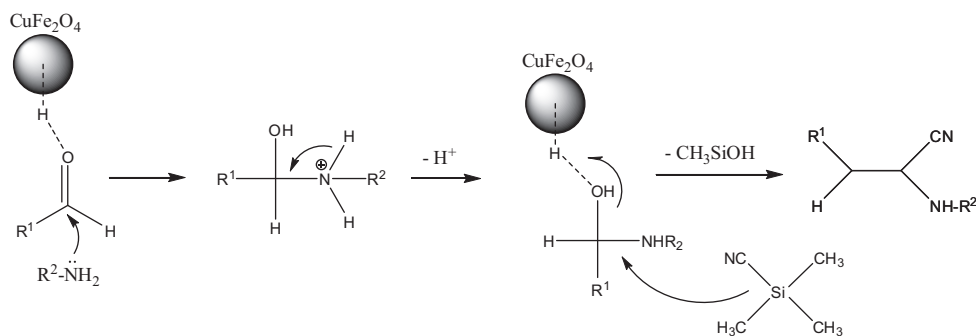
Figure 9 Suggested mechanism for the synthesis of α-aminonitriles derivatives in the presence of acidic nano copper ferrite.

| $ZnFe_2O_4$ (Zn^{2+} ions are located inside tetrahedrons). | $NdFeO_3$ (Fe^{3+} ions are located inside octahedrons). | $ZnNd_2O_4$ (Zn^{2+} ions are located inside octahedrons). |

Figure 10 The crystalline structures of $ZnFe_2O_4$ (spinel type), $NdFeO_3$ (perovskite type) and $ZnNd_2O_4$ (K_2NiF_4 type).
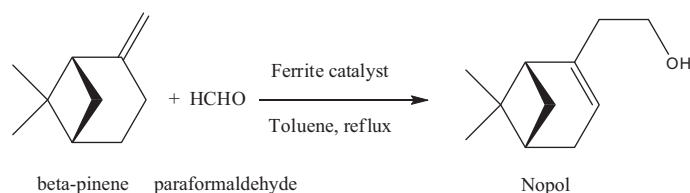
Figure 11 Prins condensation reaction of β-pinene and paraformaldehyde.
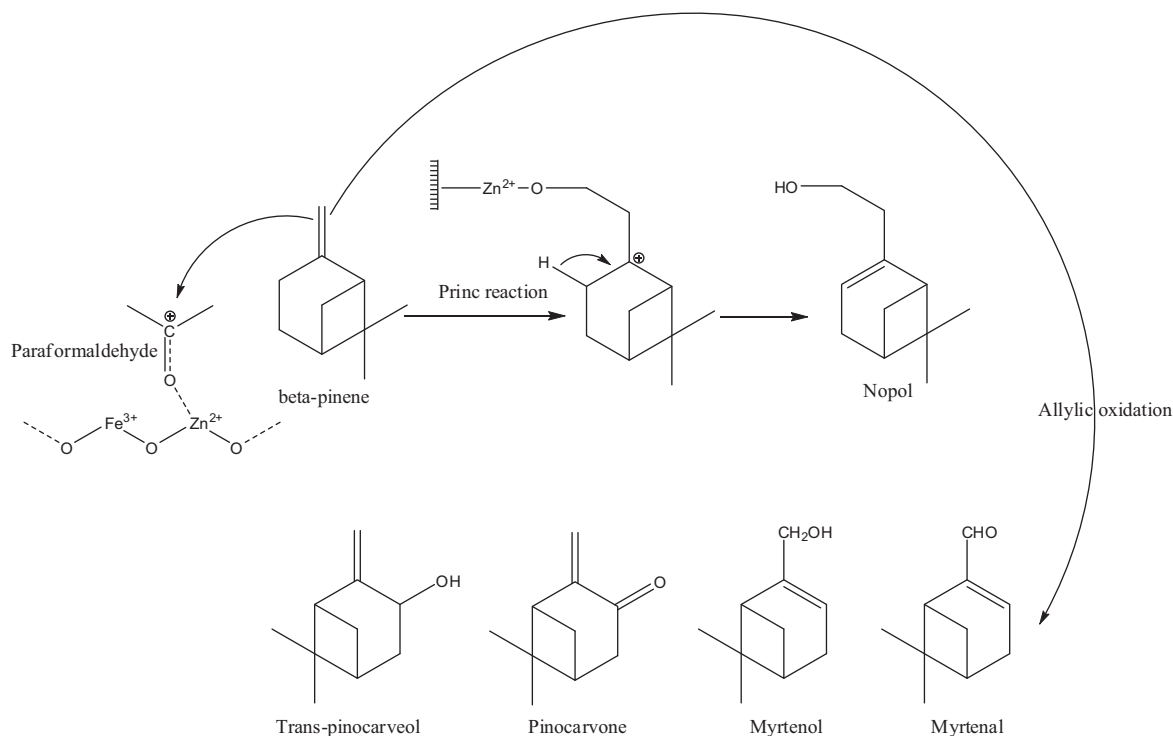
Figure 12 Proposed reaction mechanism of Prins condensation reaction for nopol production over SZF-470 catalyst.

In the case of reaction temperature, as the temperature increased to 110 °C β-pinene conversion increased to 72% with slight drop in selectivity for nopol (57%). 95 °C was identified as the optimal reaction temperature for further studies. At a molar ratio of β-pinene to paraformaldehyde 1:3 M ratio, maximum conversion was observed. The β-pinene conversion increased with an increase in the catalyst loading (0.12–0.16 g) without affecting the nopol selectivity.

Zinc ferrite nanopowders in a broader-size range (5–45 nm in size, depending on the annealing temperature) were prepared by the co-precipitation method from the corresponding nitrate pre cursors and thermal treating of the obtained precursor at different temperatures (Koleva et al., 2013). The obtained ferrites were tested as catalysts in methanol decomposition to CO and hydrogen (see also Co/Cu mixed ferrites below, applied for the same purpose). It is known that methanol, which is considered as ideal alternative green fuel for fuel cells because of its liquid state at ambient conditions and high volumetric energy density, can be decomposed to CO and H_2 at relatively low temperatures in the presence of suitable catalysts of high efficiency. The analyses of the samples after the catalytic test reveal a significant phase transformation of the ferrite phase by the influence of the reaction medium.

6. Mixed-metal or core–shell ferrites

Ferrites containing 2 metal ions, in addition to iron, are much more widespread in the nano-catalysis; their nanoparticle size can vary in a broad range, from ultrasmall particles (5–8 nm) up to 100 nm or more (in case of supported NPs). Both nano-sized and out-of-nano-sized mixed-metal ferrite NPs can be synthesized by a variety of methods, in particular the classic sol-gel and co-precipitation methods or microwave heating ($MnZnFe_2O_4$) (Zhenyu et al., 2007).

6.1. Cobalt-based ferrite nanoparticles

For cobalt-containing ferrite NPs, as well as for zinc ferrite above, one of the important applications is the methanol decomposition to CO and hydrogen. Thus, $Cu_{1-x}Co_xFe_2O_4$ ($0 < x < 1$, 8–40 nm in size), was applied as a nanodimensional powder for this purpose (Velinov, 2013). The stabilization of the cubic structure with the substitution of copper ions by cobalt in mixed Cu–Co ferrites was observed. Cobalt containing ferrites exhibited higher and more stable catalytic activity and selectivity in methanol decomposition to CO and

hydrogen in comparison with the $CuFe_2O_4$ one. Photocatalytic properties of the cobalt zinc ferrite $Co_{1-x}Zn_xFe_2O_4$ ($0 < x < 1$) nanoparticles (10.5–14.8 nm in size), prepared by the hydrothermal method, were studied on the example of degradation of methyl blue in aqueous solution (Wang, 2014). It was elucidated that the oxidation–reduction potential of methyl blue in aqueous solution in the presence of the ferrite nano-particles at pH = 7 under natural sunlight irradiation was negative and increased with an increase in Zn content. The degradation rate of methyl blue also decreases with an increase in Zn content in sunlight.

For the same purpose, $CoFe_2O_4@SiO_2@TiO_2$ core–shell magnetic nanostructures (40–100 nm in size) were prepared (Fig. 13) by coating of cobalt ferrite nanoparticles with the double SiO_2/TiO_2 layer using metal salts and titanium butoxide as precursors (Greene et al., 2014) and the presence of both the silica and very thin TiO_2 layers was confirmed. These core–shell nanoparticles were used as a catalyst in photo-oxidation reactions of methylene blue under UV light. Despite the additional non-magnetic coatings resulting in a lower value of the magnetic moment, the particles can still easily be retrieved from reaction mixtures by magnetic separation (Fig. 14). Similar (but without SiO_2 shell) $CoFe_2O_4/TiO_2$ (150 nm in size), as well as pure cobalt ferrite $CoFe_2O_4$ (50 nm in size), nanocatalysts

were prepared by the co-precipitation method, in which $CoFe_2O_4$ induced the formation of a thermodynamically more stable rutile phase of TiO_2 (Sathishkumar et al., 2013). The presence of Co^{2+} and Fe^{3+} cations on the surface of TiO_2 led to visible light absorption in the wavelength range 550–650 nm. The photocatalytic degradation of Reactive Red 120 (RR120) was studied by varying its concentration and the amount of nano-catalyst in order to attain a maximum degradation. Further, to enhance the photocatalytic degradation of RR120, electron acceptors such as peroxomonosulfate (PMS), peroxodisulfate (PDS) (Fig. 15) and hydrogen peroxide (H_2O_2) were individually added to the photocatalytic suspension at the optimized concentration of RR120 and $CoFe_2O_4/TiO_2$ nanocatalyst and their enhancing effects were studied.

6.2. Nickel-based ferrite nanoparticles

Similar to cobalt ferrites, several nickel-containing mixed or core–shell ferrites have been reported as nanocatalysts, but in a more narrow size range (18–50 nm). Thus, a magnetically separable catalyst consisting of ferric hydrogen sulfate (FHS) supported on silica-coated nickel ferrite nanoparticles (50 nm) was prepared (Fig. 16) (Khojastehnezhad et al., 2014). This catalyst
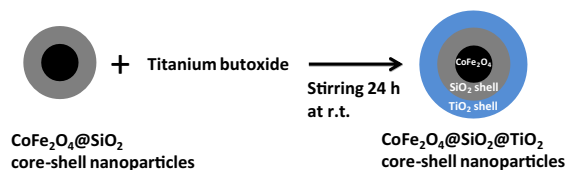
Figure 13 Reaction scheme for the coating of SiO_2 coated cobalt ferrite nanoparticles with a second TiO_2 coating.

Figure 14 Images of suspended $CoFe_2O_4@SiO_2@TiO_2$ in methylene blue solution in water (*left*) and in the presence of a permanent magnet (*right*).
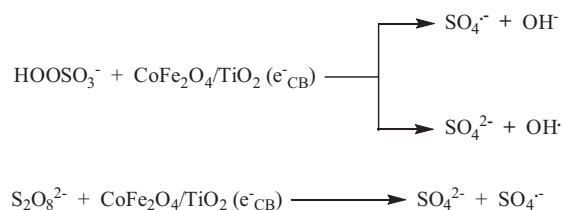
Figure 15 PMS and PDS as a source of free radicals.
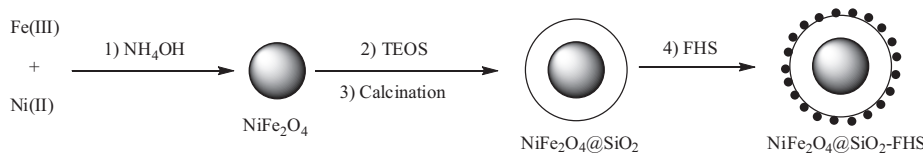
Figure 16 Preparation of NiFe$_2$O$_4$@SiO$_2$-FHS.

R = C$_6$H$_5$, 4-MeC$_6$H$_4$, 4-MeOC$_6$H$_4$
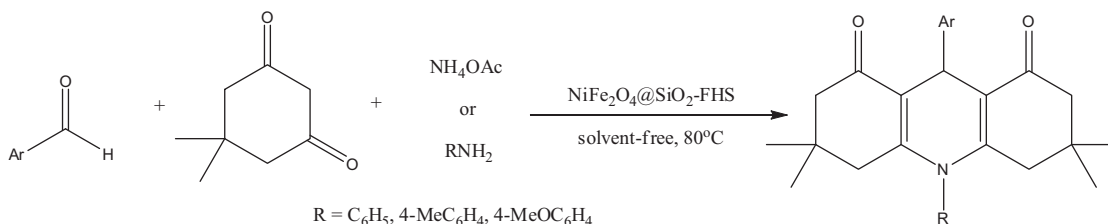
Figure 17 Synthesis of 1,8-dioxodecahydroacridines in the presence of NiFe$_2$O$_4$@SiO$_2$-FHS.

was shown to be an efficient heterogeneous catalyst for the synthesis of 1,8-dioxodecahydroacridines (Fig. 17) under solvent-free conditions. The catalyst can be recycled several times with no significant loss of catalytic activity.

Nickel–zinc ferrite nanoparticles (18–28 nm), Ni$_{1−x}$Zn$_x$Fe$_2$O$_4$ (x = 0, 0.2, 0.5, 0.8, 1.0) were prepared by a combination of chemical precipitation and spark plasma sintering (SPS) techniques and conventional thermal treatment of the obtained precursors (Velinov et al., 2012). A strong effect of reaction medium leading to the transformation of ferrites to a complex mixture of different iron containing phases was detected. A tendency of formation of iron carbide Fe$_3$C was found for the samples prepared by SPS, while predominantly iron-nickel alloys were detected in TS (thermal synthesis) obtained samples. The catalytic activity and selectivity in methanol decomposition to CO and methane (as well as for pure nickel ferrite described above, synthesized by chemical precipitation and subsequent mechanical high-energy ball milling) in a flow reactor depended on the current phase composition of the obtained ferrites, which was formed by the influence of the reaction medium. The highest activity and selectivity to CO formation was observed for monocomponent ferrites obtained by the SPS technique. Similar compound, Ni$_{0.5}$Zn$_{0.5}$Fe ferrite (crystallite size of 29 nm) doped with 0.1 and 0.4 mol.% of Cu^{2+}, was used as a catalyst for the transesterification of soybean oil to biodiesel, using methanol (Dantas, 2013). The best conversion result was obtained with nanoferrite doped with 0.4 mol.% of Cu^{2+}.

6.3. Other mixed-metal ferrite nanoparticles

Ferrite nanoparticles, containing other metals and applied in the catalysis, are represented more chaotically in the available literature. Thus, the spinel ferrites Cu$_{1−x}$Cd$_x$[Fe$_{1−x}$Al$_x$Cr$_{1−x}$Mn$_x$]O$_4$, where $0 < x < 1$, having an unknown particle size, were prepared by the coprecipitation technique (Kumar et al., 2010). Catalytic studies using decomposition of H$_2$O$_2$ as a model reaction between 303 and 343 K for 1–5 h using first order rate law suggested higher catalytic power for the composition $x = 0$ and then it decreases gradually. For the mixed spinel ferrite system Mn$_{1−x}$Cu$_x$Fe$_2$O$_4$ (x = 0, 0.25, 0.5, 0.75, 1.0), the formation of phase pure spinels with FCC cubic structure

with a particle size ranging from 5.21 nm to 20 nm was observed at 333 K applying the co-precipitation method with MnCl$_2$, Fe(NO$_3$)$_3$·9H$_2$O and Cu(NO$_3$)$_3$·3H$_2$O as precursors (Dixit et al., 2013). These ferrites were used as catalysts in the alkylation of aniline, showing a maximum conversion of 80.5% of aniline with selectivity of 98.6% toward N-methylaniline at 673 K, methanol: aniline molar ratio of 5:1 and weight hour space velocity of 0.2 h^{-1}. It was found that the yield was maximum for CuFe$_2$O$_4$. In addition, the catalytic performance of the ferrites was found to be proportional to surface area as well as acidity.

Three ferrite nanocatalysts (25–70 nm), copper ferrite (CuFe$_2$O$_4$), ferrite where cobalt was substituted by nickel (Ni$_x$Co$_{1−x}$Fe$_2$O$_4$, with x = 0, 0.2, 0.4, 0.6), and ferrite where nickel was substituted by zinc (Zn$_y$Ni$_{1−y}$Fe$_2$O$_4$ with y = 1, 0.7, 0.5, 0.3), were prepared by the sol-gel method (Hosseini Akbarnejad et al., 2013). Carbon nanotubes (CNTs) were grown on these nanocatalysts by the catalytic chemical vapor deposition method. It was revealed that the catalytic activity of these nanocrystals on the CNTs growth depend on cation distributions in the octahedral and tetrahedral sites, structural isotropy, and catalytic activity due to cations. The yield of fabrication of carbon nanotubes can be considered as an indirect tool to study catalytic activity of ferrites, which has the following order: Ni$_{0.6}$Co$_{0.4}$Fe$_2$O$_4$ > Ni$_{0.4}$Co$_{0.6}$Fe$_2$O4 > Ni$_{0.2}$Co$_{0.8}$Fe$_2$O$_4$ > CoFe$_2$O$_4$ > CuFe$_2$O$_4$ > Zn$_{0.5}$Ni$_{0.5}$Fe$_2$O$_4$ > ZnFe$_2$O$_4$ > Ni$_{0.7}$Zn$_{0.3}$Fe$_2$O$_4$ > Ni$_{0.3}$Zn$_{0.7}$Fe$_2$O$_4$. Hence, the catalytic activity of the Ni/Co ferrites increases with the increase in the Ni content due to higher catalytic activity of Ni compared to Co. In the Ni/Zn ferrites, the structural isotropy is an effective factor for their catalytic activity. The catalytic activity of Cu ferrite is higher than the Ni/Zn ferrites since it is inverse spinel, and less than Ni/Co ferrites as a result of the catalytic activity due to cations.

Selected examples of main applications of ferrites in catalysis are shown in Table 2.

7. Structure/property/particle size studies

A lot of efforts of researchers have been dedicated to establish relationships between particle size, structure, surface area, and

Table 2 Selected examples of main applications of ferrites in catalytic processes.

Catalyst composition	Process description	Process peculiarities or advantages	References
Copper ferrites			
$CuFe_2O_4$	One pot synthesis of 9-substituted aryl-1,8-dioxo-octahydroxanthenes	Excellent yields, mild reaction conditions and short reaction times	Murthy et al., 2014
$CuFe_2O_4$	Direct C–H amination of benzothiazoles	Access to a wide range of 2-*N*-substituted benzothiazoles in good to excellent yields	Satish, 2014
Nickel ferrites			
$NiFe_2O_4$	Cyanation of aryl and heteroaryl halides	Good to excellent yields	Matloubi et al., 2014
$NiFe_2O_4$	Chemoselective oxidation of thiols to disulfides and sulfides to sulfoxides	Reusable for five consecutive runs without appreciable change in the activity	Kulkarni et al., 2014
Zinc ferrites			
$ZnFe_2O_4$	Wet peroxide oxidation of 4-chlorophenol	Only a small amount of the oxidant (1 mL) is required for the complete degradation of 4-chlorophenol. 100% of the target pollutant was removed at catalyst concentrations of 300 mg	Kurian et al., 2014
$ZnFe_2O_4$	Photocatalytic dye {Reactive Red 198 (RR198) and Reactive Red 120 (RR120)} degradation ability from colored wastewater	Inorganic anions (nitrate and sulfate anions) were detected as dye mineralization products	Mahmoodi et al., 2013
Cobalt ferrites			
MFe_2O_4 (M = Mn, Co)	Degradation of Methylene Blue	Maximum MB removal achieved 99.7%, among which $>$46.8% were completely degraded	Liu et al., 2014
$CoFe_2O_4$/carbon	Methanol decomposition	After catalysis, a complex mixture of nonchanged ferrite, magnetite, Co-Fe alloy and/or Fe_3C was formed	Genova et al., 2014
Other stoichiometric ferrites			
$MnFe_2O_4$	Synthesis of spirooxindoles	One-pot and three-component reaction of isatins, malononitrile, and anilinolactones	Ghahremanzadeh, 2014
$MnFe_2O_4$ nanotubes, nanospheres and hausmannite nanorods	Potential application in peroxidase-like catalytic activity	Magnetic hollow nanotubes	Liao et al., 2011
$BiFeO_3$	Degradation of phenolic compounds	Degradation of 4-chlorophenol (4-CP), 2,4,6-trichlorophenol (2,4,6-TCP), biphenyl (BP), 4-nitrophenol (4-NP), 2,4-dinitrophenol (2,4 DNP) and 2,4,6-trinitrophenol (2,4,6-TNP)	Soltani et al., 2014
$CaFe_2O_4$	Electrocatalyst for Oxygen Evolution Reaction (OER).	Nanoparticles with irregular crystal morphology ranging from 8 to 30 nm.	Berchmans et al., 2011
$MgFe_2O_4$ (as a part of Fe_2O_3/MgO systems)	H_2O_2 decomposition.	Catalysts prepared by the hydrothermal method were most active in H_2O_2 decomposition	El-Molla et al., 2013
Mixed/doped/coated ferrites and their nanocomposites			
$CoMn_{0.2}Fe_{1.8}O_4$	Reduction of nitroaromatic compounds	Almost 100% selectivity and 100% conversions for various amino, bromo, chloro and Me derivatives of nitroarenes	Goyal et al., 2014
($Co_{0.6}Zn_{0.4}Mn_xFe_{2-x}O_4$, x = 0.2, 0.4, 0.6, 0.8 and 1.0	Photo-catalytic degradation of methyl orange azo dye	Degradation of methyl orange dye was enhanced with increase in Mn^{3+} ions concentration from 0.2 to 1.0	Bhukal et al., 2014
$ZnFe_2O_4$/SnO_2	Bactericidal activity	Saturation magnetization of hydrothermally prepared nanocomposite is less than that of sonochemically obtained one	Karunakaran et al., 2013

Table 2 (*Table continued*)

Catalyst composition	Process description	Process peculiarities or advantages	References
Metal (M)-modified ferrite catalysts (M = Cr, Al, Mn, Ce, Ni, Co and Cu)	High temperature water gas shift reaction	Fe–Al–Cu catalyst with Fe/Al = 10 and Fe/Cu = 5 wt. ratios showed the highest catalytic activity	Meshkani et al., 2015
$NiLa_xFe_{2-x}O_4$ ($0.00 \leqslant x \leqslant 2.00$)	H_2O_2 decomposition at 35–55°	A synergic effect was observed for the catalysts having x-value of 1.00 and 1.50	Abu-Zied et al., 2012
$Ru(0)/SiO_2\text{-}CoFe_2O_4$	Hydrolysis of ammonia-borane	$Ru(0)/SiO_2\text{-}CoFe_2O_4$ provides the highest catalytic activity after the tenth use in hydrolysis of AB as compared to the other ruthenium catalysts.	Akbayrak et al., 2014
Nickel hydroxide coated nanocobalt ferrite	Alcohol oxidation	Oxidation of primary and secondary alcohols efficiently (87%) to corresponding carbonyls in good yields	Bhat et al., 2014
$BiFeO_3/Ag$ (BFO/Ag)	Photocatalytic degradation of Methylene Blue	Ag NPs-decorated BFO particulates and fibers significantly shortened the degradation by 2 h as compared to their parent BFO nanostructures	Mohan et al., 2014

shape of ferrite nanoparticles, as well as nature and ratio of main and doping metal atoms, and their catalytic activity. On their basis, several interesting observations have been made. Thus, 3–10 nm Co, Cu, and Ni spinel ferrites evaluated by the decomposition of H_2O_2 and by the oxidation of methylene blue, were monitored via UV–Vis spectrophotometry (Albuquerque et al., 2012). The presence of Co^{2+} is a crucial factor required to achieve a systematic efficiency of the catalyst in the H_2O_2 decomposition. In contrast, Cu ferrites presented the better performance in methylene blue oxidation, which can be attributed to the different redox properties of Cu and the easier availability of electrons to participate in the oxidation of organic compounds. The same dye, as a classic model compound to evaluate activities of novel catalysts, was decomposed by a series of stoichiometric and non-stoichiometric cobalt and other metal ferrites. Thus, monodisperse cubic spinel structure $CoFe_2O_4$ nanoparticles (2–6 nm) showed catalytic activity in the oxidation of methylene blue with H_2O_2 as an oxidizing agent (Feng et al., 2013). 3D flower-like $Co_{3-x}Fe_xO_4$ ferrite hollow spheres (specific surface area 163 m^2/g, providing which provided more active sites) were found to be efficient for the catalytic degradation of methylene blue in the presence of H_2O_2 at 80 °C (Hao et al., 2013). In addition, in case of spinel $MgFe_2O_4$, $ZnFe_2O_4$ and orthorhombic $CaFe_2O_4$, photocatalytic performance was found to be affected by surface area and crystallinity of the photocatalyst (Dom et al., 2011). The density functional theory (DFT) calculations of MFe_2O_4 (M = Mg, Ca, Zn) lattices revealed that M-ion controllably affects the density of states of the Fe-d orbitals near Fermi level. Consequently they play an important role in determining the band-energetics and thus the visible light photocatalytic activity for methylene blue degradation.

Other dyes are also studied as model compounds in the elucidation of influence of ferrite compositions on their catalytic activity. Thus, replacement of Fe^{3+} ions by the Mn^{3+} ions in Co–Zn ferrites ($Co_{0.6}Zn_{0.4}Mn_xFe_{2-x}O_4$, x = 0.2, 0.4, 0.6, 0.8 and 1.0), possessing cubic spinel structure with Fd-3 m space groups, resulted that the degradation of methyl orange dye was enhanced with an increase in Mn^{3+} ions concentration from 0.2 to 1.0 (Bhukal et al., 2014a,b). This might be due to the octahedral site preference and higher redox potential of manganese ion as compared those of Fe. For related cobalt–zinc ferrites having chemical formula $Co_{0.6}Zn_{0.4}Cu_{0.2-}Cd_xFe_{1.8-x}O_4$ (x = 0.2, 0.4, 0.6 and 0.8), the photocatalytic degradation of methyl orange was enhanced as the concentration of cadmium ion increased from 0.2 to 0.8 which may be due to a decrease in band gap with an increase in Cd^{2+} ion concentration (Bhukal et al., 2014a,b, pp.150–158). Also, comparing with pure BFO ($BiFeO_3$) nanoparticles, the BFO/γ-Fe_2O_3 samples exhibited significantly increased visible-light photocatalytic ability toward Rhodamine B (Guo et al., 2011). The formation of a heterojunction structure between the BFO and γ-Fe_2O_3 phases was proposed to be responsible for the enhanced photocatalytic activity.

Mixed-metal ferrites have been studied also in classic reactions of oxidation and combustion of organic compounds. Thus, for Ni-doped spherical 4–6 nm $CoFe_2O_4$ nanoparticles, the $Co_{0.4}Ni_{0.6}Fe_2O_4$ with highest surface area (154.02 $m^2\ g^{-1}$) showed the best catalytic activity for reduction of 4-nitrophenol to 4-aminophenol in the presence of $NaBH_4$ as reducing agent, whereas stoichiometric $CoFe_2O_4$ was found to be catalytically inactive (Singh et al., 2014). Related nanocrystalline

$Ni_{0.5}Cu_{0.5}Fe_2O_4$ was synthesized by the sol-gel method with varying calcination temperature over the range of 500–1000 °C (Tan et al., 2011). Its single cubic spinel was gained when the precursor was decomposed at 800–1000 °C, whereas separated crystal CuO formed when calcination temperature was < 800 °C. The increase of calcination temperature favored the appearance of Fe_B^{3+}, Cu_A^{2+} and O on the spinel surface. The hydroxylation activity is relative to the amount of Cu_B^{2+} species on the spinel surface. The lattice oxygen species on the spinel surface are favorable for the deep oxidation of phenol. For nanograined $Ni_{0.5}Co_{0.5}Sc_xFe_{2-x}O_4$ (x = 0, 0.05, 0.1 and 0.2) spinel ferrites, already mentioned above, the partial substitution of Fe^{3+} by Sc^{3+} ions on the octahedral sites of spinel structure of $Ni_{0.5}Co_{0.5}Fe_2O_4$ ferrite has a favorable effect on its activity in the catalytic combustion of acetone, propane and benzene (Rezlescu et al., 2014a; Rezlescu et al., 2014b). The enhancement of the catalytic activity of the Sc doped Ni–Co ferrites may be ascribed to smaller crystallite sizes (35–39 nm), larger specific surface areas (29–32 m^2/g) and the presence of Sc cations in spinel structure. The same authors compared Mg spinel ferrite and La–Pb–Mg–Mn–O perovskite in flameless combustion reaction of acetone, benzene and propane at atmosphere pressure and revealed that a higher catalytic activity of the perovskite catalyst may be ascribed to smaller crystallite size (26 nm), larger surface specific area (8.6 m^2/g) and the presence of manganese cations with variable valence (Mn^{3+}–Mn^{4+}) (Rezlescu et al., 2014a; Rezlescu et al., 2014b).

8. Conclusions

Transition metal ferrite nanoparticles, utilized in catalytic reactions, possess different sizes, from ultrasmall 2 nm to 100 nm. They are obtained mainly by wet-chemical sol-gel (Rezlescu et al., 2014a,b) or co-precipitation (Mahmoodi et al., 2011) methods, sometimes combined with simple calcination at high temperatures (Deng et al., 2013), the sonochemical technique (Karaoglu and Baykal, 2014), mechanical (mechanochemical) high-energy ball milling (Manova et al., 2011a,b), or spark plasma sintering (Manova et al., 2011a,b). Microwave heating (Liu and Lin, 2012) or hydrothermal route (Zhang et al., 2014) are also frequently used. Sometimes, self-combustion techniques are applied (Sutka and Mezinskis, 2012; Xue et al., 2007; Rezlescu et al., 2013; Kurian and Nair, 2014; Tong et al., 2014). Due to magnetic properties, ferrite nano catalysts can be easily recovered from reaction systems and reused up to several runs almost without loss of catalytic activity. Standard transition metal salts (usually nitrates) are used as precursors, although some industrial wastes (Rashad et al., 2012) can also serve as a source of initial substances. Particle sizes of resulted spinel ferrites are dependent on the nature of transition metal and the synthesis method. A series of distinct shapes for ferrite nanoparticles have been observed, from spherical to nanorods and nanotubes. Forms/shapes of nanoparticles, ratios of doping atoms, impurities, specific surface area, etc., can considerably influence on the catalytic activity of ferrites.

Catalytic processes with the application of ferrite nanoparticles are in a wide range. Growth of carbon nanotubes is the only example of allotrope formation (Tsujino et al., 2013; Hosseini Akbarnejad et al., 2013). Notable attention is paid to methanol decomposition to CO and methane or to CO and hydrogen. Other catalyzed organic reactions consist of oxidation of various alkenes, aldol, alkylation and dehydrogenation reactions, synthesis of various organic compounds such as, quinoxaline derivatives (Dandia, 2013), β,γ-unsaturated ketones, arylidene barbituric acid derivatives, α-aminonitriles, nopol, 1,4-dihydropyridines, and 1,8-dioxodecahydro-acridines. Degradation/decomposition processes are also reported, for instance decomposition of H_2O_2 or photocatalytic degradation of Reactive Red 120 or methylene blue. Some of catalyzed reactions might have great practical applications, for instance transesterification of soybean oil to biodiesel.

We note that the total number of nano-ferrite applications for catalytic purposes is still relatively low, so it could be a perfect research niche for further applications of ferrite nanomaterials in a variety of organic processes.

References

Abbaspour, A., Mirahmadi, E., 2013. Electrocatalytic hydrogen evolution reaction on carbon paste electrode modified with Ni ferrite nanoparticles. Fuel 104, 575–582.

Abu-Zied, B. et al, 2012. Urea-based combustion process for the synthesis of nanocrystalline Ni–La–Fe–O catalysts. J. Nanomater., 428643, pp. 7.

Akbayrak, S. et al, 2014. Ruthenium(0) nanoparticles supported on magnetic silica coated cobalt ferrite: reusable catalyst in hydrogen generation from the hydrolysis of ammonia-borane. J. Mol. Catal. A: Chem. 394, 253–261.

Albuquerque, A. et al, 2012. Nanostructured ferrites: structural analysis and catalytic activity. Ceram. Int. 38 (3), 2225–2231.

Berchmans, L.J. et al, 2011. Mechanochemical synthesis and electrochemical characterization of nano crystalline calcium ferrite. Catal. Lett. 141 (10), 1451–1457.

Bhat, P. et al, 2014. Nickel hydroxide/cobalt–ferrite magnetic nanocatalyst for alcohol oxidation. ACS Comb. Sci. 16 (8), 397–402.

Bhukal, S. et al, 2014a. Magnetic Mn substituted cobalt zinc ferrite systems. Structural, electrical and magnetic properties and their role in photo-catalytic degradation of methyl orange azo dye. Physica B 445, 48–55.

Bhukal, S. et al, 2014b. $Co_{0.6}Zn_{0.4}Cu_{0.2}Cd_xFe_{1.8-x}O_4$ (0.2 ≤ x ≤ 0.8) magnetic ferrite nano-particle: synthesis, characterization and photo-catalytic degradation of methyl orange. J. Mol. Struct. 1059, 150–158.

Dandia, A., Singh, R., Joshi, J., Maheshwari, S., 2013. Magnetically separable CuFe2O4 nanoparticles: an efficient catalyst for the synthesis of quinoxaline derivatives in tap-water under sonication. Eur. Chem. Bull. 2 (10), 825–829.

Dantas, J., 2013. Use of Ni–Zn ferrites doped with cu as catalyst in the transesterification of soybean oil to methyl esters. Mater. Res. 16 (3), 625–627.

Deng, J. et al, 2013. $CoFe_2O_4$ magnetic nanoparticles as a highly active heterogeneous catalyst of oxone for the degradation of diclofenac in water. J. Hazard. Mater. 262, 836–844.

Dixit, R. et al, 2013. Methylation of aniline over Mn–Cu ferrites catalysts. Global J. Sci. Front. Res. Chem. 13 (7), 10.

Dom, R. et al, 2011. Synthesis of solar active nanocrystalline ferrite, MFe_2O_4 (M: Ca, Zn, Mg) photocatalyst by microwave irradiation. Solid State Commun. 151 (6), 470–473.

El-Molla, S. et al, 2013. Effect of the method of preparation on the physicochemical and catalytic properties of nanosized Fe_2O_3/MgO. Res. Chem. Intermed. (Ahead of Print).

Feng, X. et al, 2013. Controlled synthesis of monodisperse $CoFe_2O_4$ nanoparticles by the phase transfer method and their catalytic activity on methylene blue discoloration with H_2O_2. J. Magn. Magn. Mater. 343, 126–132.

Gaikwad, R.-S. et al, 2011. Cobalt ferrite nanocrystallites for sustainable hydrogen production application. Int. J. Electrochem., 6, 729141.

Gatelite, A. et al, 2011. Sol-gel synthesis and characterization of selected transition metal nano-ferrites. Mater. Sci. (MEDŽIAGO-TYRA) 17 (3), 302–307.

Genova et al., 2014. Cobalt ferrite nanoparticles hosted in activated carbon from renewable sources as catalyst for methanol decomposition. Catal. Commun. 55, 43–48.

Ghahremanzadeh, R. et al, 2014. Manganese ferrite nanoparticle catalyzed tandem and green synthesis of spirooxindoles. RSC Adv. (Ahead of Print).

Gharib, A. et al, 2014. Catalytic synthesis of α-aminonitriles using nano copper ferrite ($CuFe_2O_4$) under green conditions. Org. Chem. Int., 8, 169803.

Goodarz Naseri, M. et al, 2010. Simple synthesis and characterization of cobalt ferrite nanoparticles by a thermal treatment method. J. Nanomater., 8, 907686.

Goyal, A. et al, 2014. $CoMn_{0.2}Fe_{1.8}O_4$ ferrite nanoparticles engineered by sol–gel technology: an expert and versatile catalyst for the reduction of nitroaromatic compounds. J. Mater. Chem. A 2, 18848–18860.

Greene, D. et al, 2014. Synthesis characterization and photocatalytic studies of cobalt ferrite–silica–titania nanocomposites. Nanomaterials 4, 331–343.

Guo, R. et al, 2011. Magnetically separable $BiFeO_3$ nanoparticles with a γ-Fe_2O_3 parasitic phase: controlled fabrication and enhanced visible-light photocatalytic activity. J. Mater. Chem. 21 (46), 18645–18652.

Hao, J. et al, 2013. Hierarchical flower-like $Co_{3-x}Fe_xO_4$ ferrite hollow spheres: facile synthesis and catalysis in the degradation of Methylene Blue. Nanoscale 5 (7), 3078–3082.

Hong, D. et al, 2012. Catalysis of nickel ferrite for photocatalytic water oxidation using $[Ru(bpy)_3]^{2+}$ and $S_2O_8^{2-}$. J. Am. Chem. Soc. 134, 19572–19575.

Hosseini Akbarnejad, R. et al, 2013. Catalytic activity of the spinel ferrite nanocrystals on the growth of carbon nanotubes. J. Supercond. Nov. Magn. 2013 (26), 429–435.

Jadhav, S.V. et al, 2012. Nanosized sulfated zinc ferrite as catalyst for the synthesis of nopol and other fine chemicals. Catal. Today 198, 98–105.

Kamal Senapati, K., Phukan, P., 2011. Magnetically separable cobalt ferrite nanocatalyst for aldol condensations of aldehydes and ketones. Bull. Catal. Soc. India 9, 1–8.

Karaoglu, E., Baykal, A., 2014. $CoFe_2O_4$–Pd(0) nanocomposite: magnetically recyclable catalyst. J. Supercond. Novel Magn. 27 (9), 2041–2047.

Karunakaran, C. et al, 2013. Hydrothermal and sonochemical preparation and photocatalytic and bactericidal activities of $ZnFe_2O_4$–SnO_2 nanocomposite. Superlattices Microstruct. 60, 487–499.

Kasi Viswanath, I.V. et al, 2013. Synthesis and characterization of nano ferrites by citrate gel method. Int. J. Chem. Sci. 11 (1), 64–72.

Kasi Viswanath, I.V., Murthy, Y.L.N, et al, 2013. One-pot, three-component synthesis of 1, 4-dihydropyridines by using nano crystalline copper ferrite. Chem. Sci. Trans. 2 (1), 227–233.

Kaur Rajput, J., Kaur, G., 2013. $CoFe_2O_4$ nanoparticles: an efficient heterogeneous magnetically separable catalyst for "click" synthesis of arylidene barbituric acid derivatives at room temperature. Chin. J. Catal. 34, 1697–1704.

Kharisov, B.I. et al, 2012. Iron-containing nanomaterials: synthesis, properties, and environmental applications. RSC Adv. 2 (25), 9325–9358.

Khojastehnezhad, A. et al, 2014. Ferric hydrogen sulfate supported on silica-coated nickel ferrite nanoparticles as new and green magnetically separable catalyst for 1,8-dioxodecahydroacridine synthesis. Chin. J. Catal. 35, 376–382.

Koferstein, R. et al, 2013. Preparation and characterization of nanosized magnesium ferrite powders by a starch-gel process and corresponding ceramics. J. Mater. Sci. 48, 6509–6518.

Koleva, K.V. et al, 2013. Preparation, structure and catalytic properties of $ZnFe_{24}$. Bulg. Chem. Commun. 45 (4), 434–439.

Kooti, M., Afshari, M., 2012. Magnetic cobalt ferrite nanoparticles as an efficient catalyst for oxidation of alkenes. Scientia Iranica F 19 (6), 1991–1995.

Kulkarni, A. et al, 2014. Nickel ferrite nanoparticles-hydrogen peroxide: a green catalyst-oxidant combination in chemoselective oxidation of thiols to disulfides and sulfides to sulfoxides. RSC Adv. 4 (69), 36702–36707.

Kumar, P.V., Short, M.P., Yip, S., Yildiz, B., Grossman, J.C., 2013. High surface reactivity and water adsorption on $NiFe_2O_4$ (111) surfaces. J. Phys. Chem. C 117 (11), 5678–5683.

Kumar, B., Gupta, S., Venkatachalam, A., et al, 2010. Synthesis and characterization of spinel ferrites $Cu_{1-x}Cd_x[Fe_{1-x}Al_xCr_{1-x}Mn_x]$-$O_4$. Rasayan J. Chem. 3 (4), 745–750.

Kurian, M. et al, 2014. Influence of the synthesis conditions on the catalytic efficiency of $NiFe_2O_4$ and $ZnFe_2O_4$ nanoparticles towards the wet peroxide oxidation of 4-chlorophenol- reaction kinetics. Mech. Catal. 111 (2), 591–604.

Kurian, M., Nair, D.S., 2014. On the efficiency of cobalt zinc ferrite nanoparticles for catalytic wet peroxide oxidation of 4-chlorophenol. J. Environ. Chem. Eng. 2 (1), 63–69.

Liao, M. et al, 2011. Synthesis of magnetic hollow nanotubes based on the kirkendall effect for MR contrast agent and colorimetric hydrogen peroxide sensor. J. Mater. Chem. 21 (22), 7974–7981.

Lim, Choon Woo, Lee, In Su, 2010. Magnetically recyclable nanocatalyst systems for the organic reactions. Nano Today 5, 412–434.

Liu, S. et al, 2014. Microwave-enhanced catalytic degradation of methylene blue by porous MFe_2O_4 (M = Mn, Co) nanocomposites: pathways and mechanisms. Sep. Purif. Technol. 135, 35–41.

Liu, Y.-C., Lin, C.-M., 2012. Kinetic study of the 2,3,5-trimethyl-1,4-benzoquinone synthesis in the presence of $CuFe_2O_4$ nano-powder as the catalyst. Adv. Sci. Lett. 9, 120–125.

Lou, J.-C., Chang, C.-K., 2006. Catalytic oxidation of CO over a catalyst produced in the ferrite process. Env. Eng. Sci. 23 (6), 1024–1032.

Lu, H.-C. et al, 2011. Porous ferrite synthesis and catalytic effect on benzene degradation. Int. J. Phys. Sci. 6 (4), 855–865.

Mahmoodi, N. et al, 2013. Zinc ferrite nanoparticle as a magnetic catalyst: synthesis and dye degradation. Mater. Res. Bull. 48 (10), 4255–4260.

Mahmoodi et al., 2011. Photocatalytic ozonation of dyes using copper ferrite nanoparticle prepared by co-precipitation method. Desalination 279 (1–3), 332–337.

Manova, E. et al., 2007. Mössbauer study of nanodimensional nickel ferrite – mechanochemical synthesis and catalytic properties. In: Lippens, P.-E., Jumas, J.-C., Génin, J.-M.R. (Eds.), Proceedings of the 28th international conference on the applications of the Mössbauer effect. ICAME 2005, 4–9 September 2005, vol. I (Part I-II/V), Montpellier, France. pp.215–220.

Manova, E. et al, 2011a. Nanosized copper ferrite materials: mechanochemical synthesis and characterization. J. Solid State Chem. 184 (5), 1153–1158.

Manova, E. et al, 2011b. Nanodimensional nickel–zinc ferrite $Ni_{0.5}$-$Zn_{0.5}Fe_2O_4$ – synthesis and characterization. Nanosci. Nanotechnol. 11, 138–141.

Matloubi, M. et al, 2014. Highly active recyclable heterogeneous nanonickel ferrite catalyst for cyanation of aryl and heteroaryl halides. Appl. Organomet. Chem. 28 (10), 750–755.

Meshkani, F., Rezaei, M., 2015. Preparation of nanocrystalline metal (Cr, Al, Mn, Ce, Ni, Co and Cu) modified ferrite catalysts for the high temperature water gas shift reaction. Renewable Energy 74, 588–598.

Mohan, S. et al, 2014. A prototypical development of plasmonic multiferroic bismuth ferrite particulate and fiber nanostructures and their remarkable photocatalytic activity under sunlight. J. Mater. Chem. C: Mater. Opt. Electron. Devices 2 (33), 6835–6842.

Murthy, Y.L.N. et al, 2012. Nano copper ferrite: A reusable catalyst for the synthesis of β, γ-unsaturated ketones. J. Chem. Sci. 124 (3), 639–645.

Murthy et al., 2014. Synthesis and antibacterial assay of 9-substituted aryl-1,8-dioxo-octahydroxanthenes. Asian J. Chem. 26 (15), 4594–4598.

Papa, F. et al, 2010. Catalytic behavior of neodymium substituted zinc ferrites in oxidative coupling of methane. Rev. Roum. Chim. 55 (1), 33–38.

Pinheiro Braga, T. et al, 2011. Catalytic properties of cobalt and nickel ferrites dispersed in mesoporous silicon oxide for ethylbenzene dehydrogenation with CO_2. Catal. Sci. Technol. 1, 1383–1392.

Radhakrishnan Nair, T.D., Aniz, C.U., 2013. Effect of redox nature of impregnated ferrite catalysts on their carbon monoxide oxidation activity. RRJMS 1 (2), 45–52.

Rashad et al., 2012. Magnetic and catalytic properties of cubic copper ferrite nanopowders synthesized from secondary resources. Adv. Powder Technol. 23, 315–323.

Rezlescu, N., Rezlescu, E., Popa, P.D., Doroftei, C., Ignat, M., 2013. Comparative study between catalyst properties of simple spinel ferrite powders prepared by self-combustion route. Rom. Rep. Phy. 65 (4), 1348–1356.

Rezlescu, N. et al, 2014a. Scandium substituted nickel-cobalt ferrite nanoparticles for catalyst applications. Appl. Catal. B 158–159, 70–75.

Rezlescu, N. et al, 2014b. Structural and catalytic properties of mesoporous nanocrystalline mixed oxides containing magnesium. Catal. Commun. 46, 51–56.

Santina Mohallem, N.D. et al, 2012. Study of multifunctional nanocomposites formed by cobalt ferrite dispersed in a silica matrix prepared by sol-gel process. In: Farzad, E. (Ed.), Nanocomposites – New Trends and Developments. InTech, pp. 457–482, Chapter 18).

Sathishkumar, P. et al, 2013. $CoFe_2O_4/TiO_2$ nanocatalysts for the photocatalytic degradation of Reactive Red 120 in aqueous solutions in the presence and absence of electron acceptors. Chem. Eng. J. 220, 302–310.

Satish, G. et al, 2014. Direct C–H amination of benzothiazoles by magnetically recyclable $CuFe_2O_4$ nanoparticles under ligand-free conditions. Tetrahedron Lett. 55 (40), 5533–5538.

Shen, Yu. et al, 2013. Facile preparation of sphere-like copper ferrite nanostructures and their enhanced visible-light-induced photocatalytic conversion of benzene. Mater. Res. Bull. 48 (10), 4216–4222.

Singh, C. et al, 2014. Nickel-doped cobalt ferrite nanoparticles: efficient catalysts for the reduction of nitroaromatic compounds and photo-oxidative degradation of toxic dyes. Nanoscale 6 (14), 7959–7970.

Soltani, T. et al, 2014. Solar-Fenton catalytic degradation of phenolic compounds by impure bismuth ferrite nanoparticles synthesized via ultrasound. Chem. Eng. J. 251, 207–216.

Sutka, A., Mezinskis, G., 2012. Sol-gel auto-combustion synthesis of spinel-type ferrite nanomaterials. Front. Mater. Sci. 6 (2), 128–141.

Tan, X. et al, 2011. Effect of calcination temperature on the structure and hydroxylation activity of $Ni_{0.5}Cu_{0.5}Fe_2O_4$ nanoparticles. Appl. Surf. Sci. 257 (14), 6256–6263.

Tong et al., 2014. Aerobic oxidation of cyclohexane effectively catalyzed by simply synthesized silica-supported cobalt ferrite magnetic nanocrystal. Ind. Eng. Chem. Res. 53 (25), 10294–10300.

Tsujino, G. et al, 2013. Catalytic synthesis of carbon nanotube over nickel ferrite loaded oxidized diamond catalyst. Trans. Mater. Res. Soc. Jpn 38 (3), 435–438.

Velinov, N., 2013. Copper-cobalt ferrites as catalysts for methanol decomposition. In: 11th European Congress on Catalysis – EuropaCat-XI. September 1st-6th, Lyon, France, 2013.

Velinov, N. et al, 2012. Spark plasma sintering synthesis of $Ni_{1-x}Zn_xFe_2O_4$ ferrites: Mössbauer and catalytic study. Solid State Sci. 14 (8), 1092–1099.

Wang, L.L., He, H.Y., 2014. Surface alkaline-acidic characteristics and photo catalytic properties of $Co_{1-x}Zn_xFe_2O_4$ nano-particles synthesized by hydrothermal method. J. Sci. Res. Rep. 3 (2), 263–274, JSRR.2014.001.

Xue, H., Li, Z., Wang, X., Fu, X., 2007. Facile synthesis of nanocrystalline zinc ferrite via a self-propagating combustion method. Mater. Lett. 61 (2), 347–350.

Zhang, H. et al, 2014. Copper ferrite-graphene hybrid: a highly efficient magnetic catalyst for chemoselective reduction of nitroarenes. RSC Adv. 4 (59), 31328–31332.

Zhenyu, L. et al, 2007. Microwave assisted low temperature synthesis of MnZn ferrite nanoparticles. Nanoscale Res. Lett. 2, 40–43.